

RESEARCH ARTICLE

Transcriptional repression of Myc underlies the tumour suppressor function of AGO1 in *Drosophila*

Olga Zaytseva^{1,*}, Naomi C. Mitchell^{1,*}, Linna Guo^{1,*}, Owen J. Marshall², Linda M. Parsons², Ross D. Hannan¹, David L. Levens³ and Leonie M. Quinn^{1,‡}

ABSTRACT

Here, we report novel tumour suppressor activity for the *Drosophila* Argonaute family RNA-binding protein AGO1, a component of the miRNA-dependent RNA-induced silencing complex (RISC). The mechanism for growth inhibition does not, however, involve canonical roles as part of the RISC; rather, AGO1 controls cell and tissue growth by functioning as a direct transcriptional repressor of the master regulator of growth, Myc. AGO1 depletion in wing imaginal discs drives a significant increase in ribosome biogenesis, nucleolar expansion and cell growth in a manner dependent on Myc abundance. Moreover, increased Myc promoter activity and elevated Myc mRNA in AGO1-depleted animals requires RNA polymerase II transcription. Further support for transcriptional AGO1 functions is provided by physical interaction with the RNA polymerase II transcriptional machinery (chromatin remodelling factors and Mediator Complex), punctate nuclear localisation in euchromatic regions and overlap with Polycomb Group transcriptional silencing loci. Moreover, significant AGO1 enrichment is observed on the Myc promoter and AGO1 interacts with the Myc transcriptional activator Psi. Together, our data show that *Drosophila* AGO1 functions outside of the RISC to repress Myc transcription and inhibit developmental cell and tissue growth.

This article has an associated 'The people behind the papers' interview.

KEY WORDS: Argonaute, *Drosophila*, Myc, Proliferation, Psi, Transcription

INTRODUCTION

Tightly coordinated regulation of cell and tissue growth is essential for animal development. Decreased growth leads to small organs and diminished body size, whereas heightened proliferative growth is associated with genomic instability and cancer. The MYC transcription factor and growth regulator has been studied extensively since its identification as an oncogene in the early 1980s (Vennstrom et al., 1982), when MYC overexpression caused


by chromosomal translocation was found to drive malignant transformation in Burkitt's lymphoma (Dalla-Favera et al., 1982; Taub et al., 1982). Research in subsequent decades implicated increased MYC in progression of most tumours (Dang, 2012; Liao and Dickson, 2000; Meyer and Penn, 2008). In normal adult tissues, MYC expression is relatively low and generally restricted to cells with regenerative and proliferative potential (Marcu et al., 1992). Even small increases in MYC abundance are sufficient to promote proliferative cell growth (reviewed by Dang, 2010; Levens, 2010; Zaytseva and Quinn, 2017); thus, understanding the molecular control of MYC expression can provide crucial insight into the mechanisms of MYC dysregulation in cancer.

In normal cells, MYC is regulated by signalling inputs from a diverse array of developmental and growth signalling pathways (Zaytseva and Quinn, 2017). The many cellular signalling inputs converging on MYC transcription are integrated by FUBP1, a KH domain protein that binds single-stranded DNA and interacts with the general transcription factor complex TFIID to modulate MYC promoter output (Chung and Levens, 2005; Chung et al., 2006; He et al., 2000; Liu et al., 2006; Zhang and Chen, 2013). The mammalian FUBP family comprises three proteins (FUBP1-3) (Zhang and Chen, 2013), which are represented by one orthologue in *Drosophila*, Psi. Like FUBP1, Psi also interacts with the RNA polymerase II (RNA Pol II) transcriptional machinery, particularly the transcriptional Mediator (MED) complex, to pattern Myc transcription and cell and tissue growth in the *Drosophila* wing epithelium (Guo et al., 2016). In addition to roles in transcription, Psi binds RNA via the KH domains and interacts with the spliceosome to regulate mRNA splicing (Labourier et al., 2001; Wang et al., 2016). Although co-immunoprecipitation (co-IP) mass spectrometry detected Psi in complex with the Argonaute protein AGO1 (Guo et al., 2016), the potential significance of this interaction is unknown.

Argonaute proteins comprise the core of the RNA-induced silencing complex (RISC), which uses noncoding RNA as a guide to target mRNAs for post-transcriptional gene silencing. *Drosophila* AGO2 is best characterised as part of the siRNA-induced silencing complex (siRISC) (Okamura et al., 2004), whereas AGO1 predominantly functions in microRNA-induced silencing complexes (miRISCs) and post-transcriptional mRNA silencing (Förstemann et al., 2007). Of importance to this study, AGO1-mediated mRNA silencing has been implicated in transcript destabilisation and translational repression of Myc in flies (Daneshvar et al., 2013) and humans (Challagundla et al., 2011). Here, we report a novel role for AGO1 as a direct Myc transcriptional repressor and demonstrate that this underlies cell growth inhibition. AGO1 depletion not only increases Myc promoter activity, mRNA and protein abundance, but the elevated Myc expression requires RNA Pol II transcriptional activity. Localisation to the nucleus, together with interaction with transcriptional machinery and significant AGO1 enrichment on the Myc promoter suggests, in

¹Department of Cancer Biology and Therapeutics, The John Curtin School of Medical Research, The Australian National University, Canberra, ACT 2600, Australia. ²University of Tasmania, Hobart, Tasmania 7000, Australia. ³Center for Cancer Research, National Cancer Institute, NIH, Bethesda, MD 20892, USA. *These authors contributed equally to this work

[‡]Author for correspondence (leonie.quinn@anu.edu.au)

 O.Z., 0000-0001-9684-6382; L.M.Q., 0000-0002-3911-6508

This is an Open Access article distributed under the terms of the Creative Commons Attribution License (<https://creativecommons.org/licenses/by/4.0>), which permits unrestricted use, distribution and reproduction in any medium provided that the original work is properly attributed.

Handling Editor: Haruhiko Koseki
Received 9 March 2020; Accepted 27 April 2020

addition to the established roles in miRNA silencing in the cytoplasm, AGO1 constrains *Myc* transcription to control cell and tissue growth during *Drosophila* development.

RESULTS

AGO1 interacts with Psi and RNA Pol II transcriptional machinery

The single-stranded DNA/RNA binding protein Psi has essential roles in *Myc* transcriptional control and RNA processing in *Drosophila*. In addition to physically and genetically interacting with the RNA Pol II transcriptional machinery, the *Drosophila* Protein Interaction Map (DPiM) large scale co-IP mass spectrometry (Guruharsha et al., 2011) suggested association between Psi and AGO1 (Guo et al., 2016). Our analysis of the DPiM identified Psi as the most frequent AGO1 interacting partner (Fig. 1A). Ontological class analysis for the top 70 AGO1 interactors revealed RNA processing factors (49%), as expected;

however, most (59%) interactors had ascribed functions in RNA Pol II transcription (Fig. 1A-C, note 10 factors are implicated in both transcription and RNA processing). As the DPiM studies were performed *in vitro* with overexpressed tagged proteins in *Drosophila* S2 cell lines, we validated the interaction between endogenous AGO1 and Psi *in vivo* using co-IP from wild-type third instar larval imaginal tissue. Immunoprecipitation using anti-Psi antibody, followed by anti-AGO1 western blot detected a 110 kDa band for AGO1 (Fig. 1D), whereas reciprocal IP with anti-AGO1 antibody precipitated the 97 kDa Psi band (Fig. 1E). The observation that endogenous AGO1 and Psi form a complex *in vivo* led us to investigate potential genetic interactions between AGO1 and Psi.

Psi-dependent growth is sensitive to AGO1 abundance

Psi knockdown in the dorsal wing compartment results in a ‘wings up’ phenotype as impaired cell and tissue growth of the top layer of

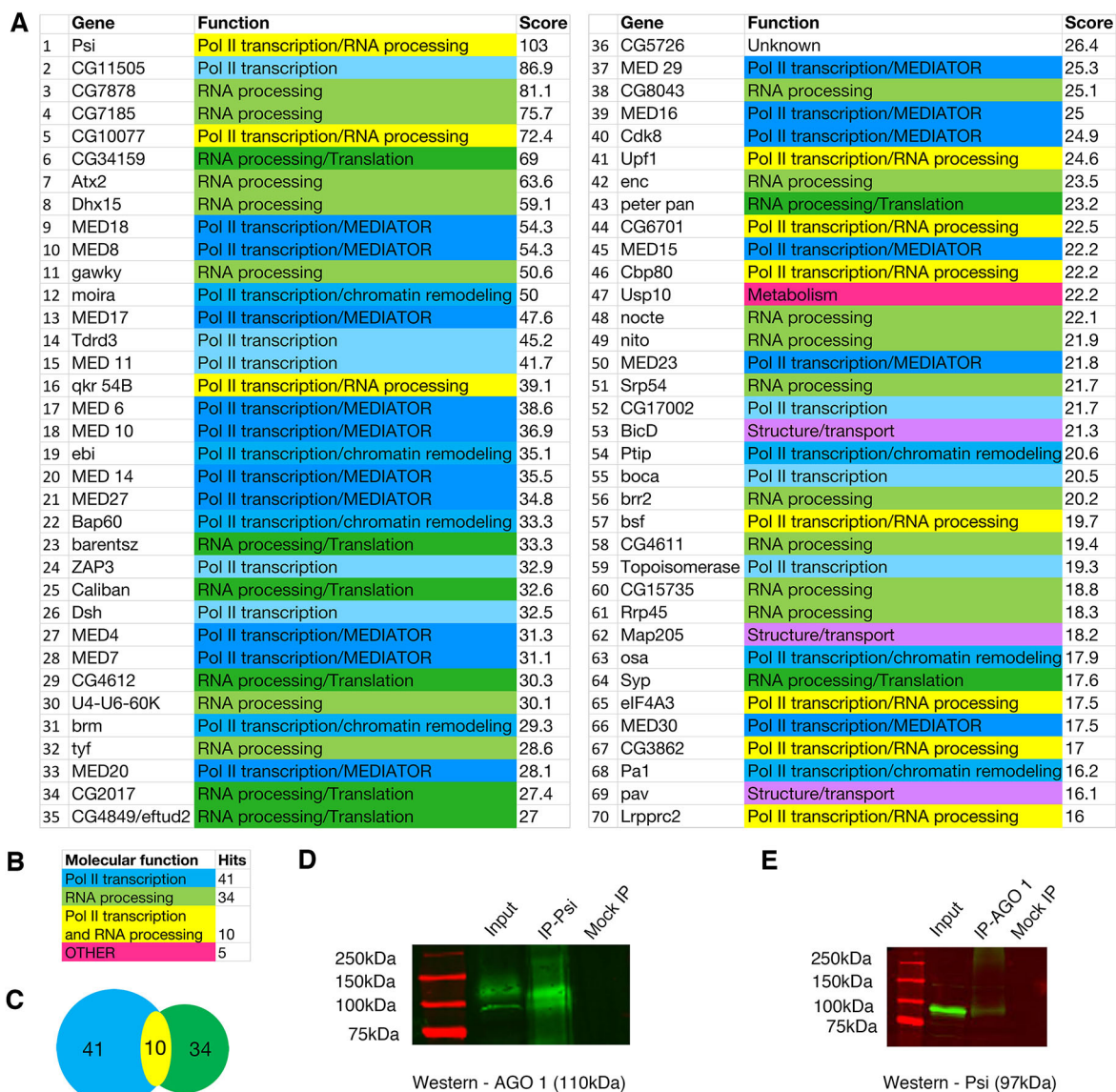


Fig. 1. AGO1 interacts with RNA Pol II transcriptional machinery and RNA processing factors. (A) List of top 70 AGO1 interactors from the *Drosophila* Protein Interaction Map (DPiM) dataset (Guruharsha et al., 2011). (B) Summary of ontology classes for the top 70 AGO1 interactors. (C) Intersection of interactors with functions in RNA Pol II transcription and/or RNA processing. (D,E) Co-IP of endogenous Psi and AGO1 from wild-type third instar larvae. (D) IP with anti-Psi and western blot with anti-AGO1 (110 kDa). (E) IP with anti-AGO1 and western blot with anti-Psi (97 kDa). Mock IP refers to no-antibody control.

the wing results in torsional strain and wing bending (Guo et al., 2016). We therefore tested whether this was modulated by AGO1 depletion, using two independent P-element insertion mutants (*AGO1^{k00208}* and *AGO1⁰⁴⁸⁴⁵*). Interestingly, *AGO1* heterozygosity alone was sufficient to increase wing size, suggesting that AGO1 normally constrains growth. Moreover, heterozygosity for either *AGO1* mutant suppressed impaired tissue growth caused by Psi depletion (Fig. 2A-C). Thus, AGO1 normally functions as a negative growth regulator and the wing overgrowth associated with AGO1 reduction is dependent upon Psi. However, we need to be somewhat cautious in our interpretation of these data as either genotype alone results in a phenotype, where the outcome may be an intermediate phenotype between the larger wings from AGO1 heterozygotes and impaired growth from Psi knockdown.

AGO1 depletion drives cell growth in a Myc-dependent manner

To further examine the cellular basis of the tissue overgrowth associated with AGO1 depletion in specific compartments of the larval wing, we used two independent non-overlapping *AGO1* RNAi lines. We first demonstrated efficient mRNA knockdown for both *AGO1* lines in the wing (Fig. S1A) and dorsal compartment-specific protein knockdown 24 h after induction of *ser-GAL4* (Fig. S1B). As pupal lethality and dorsal compartment cell death were associated with constitutive *ser-GAL4* driven AGO1 knockdown (Fig. S2), the baculoviral caspase inhibitor p35 was co-expressed to prevent apoptosis (Hay et al., 1994) and enable investigation of potential changes to cell growth.

Cell growth requires ribosomal RNA (rRNA) synthesis, processing and assembly with ribosomal proteins (RPs) into 40S and 60S ribosomal subunits in the nucleolus. Thus, the size of this structure, as measured by nucleolar-specific fibrillar antibody, provides an indirect measure of ribosome biogenesis (Mitchell et al., 2015). AGO1 depletion significantly increased nucleolar size (Fig. 3A,B), and cell size (Fig. 3C), suggesting that AGO1 normally functions to inhibit cell growth. Consistent with AGO1 depletion driving nucleolar expansion, at least in part a result of increased rDNA transcription, transient *AGO1* knockdown significantly increased pre-rRNA levels and *Polr1c* (RNA polymerase I (subunit) mRNA (Fig. 3D). AGO1 depletion also

significantly increased levels of the ribosomal protein subunits *Rps19* and *Rps24* (Fig. 3D). Together, these data suggest that AGO1 normally inhibits ribosome biogenesis and cell growth in the wing imaginal disc. Chromatin immunoprecipitation (ChIP) sequencing studies have previously identified AGO2 binding throughout the 47S region of the consensus rRNA gene in human cell lines (Atwood et al., 2016), suggesting direct roles for AGO proteins in rDNA transcription and/or rRNA processing. However, these observations do not explain the increase in expression of RNA Pol II-transcribed ribosomal proteins and RNA Pol I subunits, nor the increase in overall cell growth, which requires coordinated activity from all three RNA polymerases, RNA Pol I, II and III (the last required for transcription of 5S rRNA).

MYC drives cell growth by stimulating transcription of all three RNA polymerases to upregulate ribosome production (Poortinga et al., 2014). MYC directly stimulates the initiation of RNA Pol I-mediated transcription in mammals (Arabi et al., 2005; Grandori et al., 2005; Shiu et al., 2009) and activates transcription of RNA Pol II-transcribed genes encoding the ribosomal proteins (RPs), rRNA processing factors and components of the nucleolus essential for ribosome biogenesis (Grandori et al., 2005; Grewal et al., 2005; Poortinga et al., 2011). Furthermore, MYC directly activates RNA Pol III transcription to increase 5S rRNA expression (for assembly of the large 60S ribosomal subunit) and tRNA for translation of mRNA into protein (Fernandez et al., 2003; Gomez-Roman et al., 2006; Oskarsson and Trumpp, 2005). In *Drosophila*, Myc depletion reduced nucleolar expansion in AGO1 knockdown wing cells to the control range (Fig. 4A,B). Co-depletion of the Myc-regulator Psi also significantly decreased nucleolar size compared with AGO1 knockdown alone (Fig. 4A,B). Importantly, given the intermediate effect between *ser-GAL4* driven Psi knockdown and AGO1 heterozygotes in the adult wing (Fig. 2), Psi depletion alone did not modify nucleolar size. Thus, the increased ribosome biogenesis and cell overgrowth associated with AGO1 depletion is dependent on both Psi and Myc.

AGO1 depletion increases Myc abundance and function

The overgrowth observed in AGO1 knockdown wing imaginal disc cells (Figs 3,4) was associated with a significant increase in *Myc* mRNA, which was reduced by Psi co-knockdown (Fig. 5A). AGO1

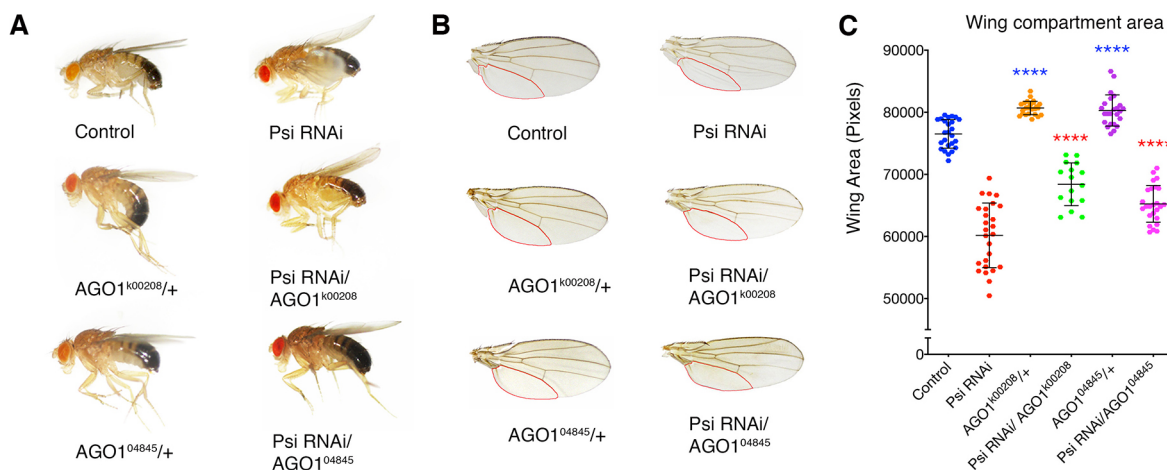


Fig. 2. Impaired cell and tissue growth in the Psi knockdown wing is sensitive to AGO1 levels. (A,B) Adult flies (A) and wings (B), with compartment below vein L5 outlined in red (genotypes in the *ser-GAL4* background as marked). (C) Quantification of compartment area below vein L5 in individual adult wings in the *ser-GAL4* background. Data points are measurements per individual wing, with mean±s.d. shown. Both *AGO1* mutants were compared with the control; *AGO1* mutants in *Psi* RNAi background were compared with *Psi* knockdown alone. Unpaired two-tailed *t*-test was used for all comparisons. *****P*<0.0001.

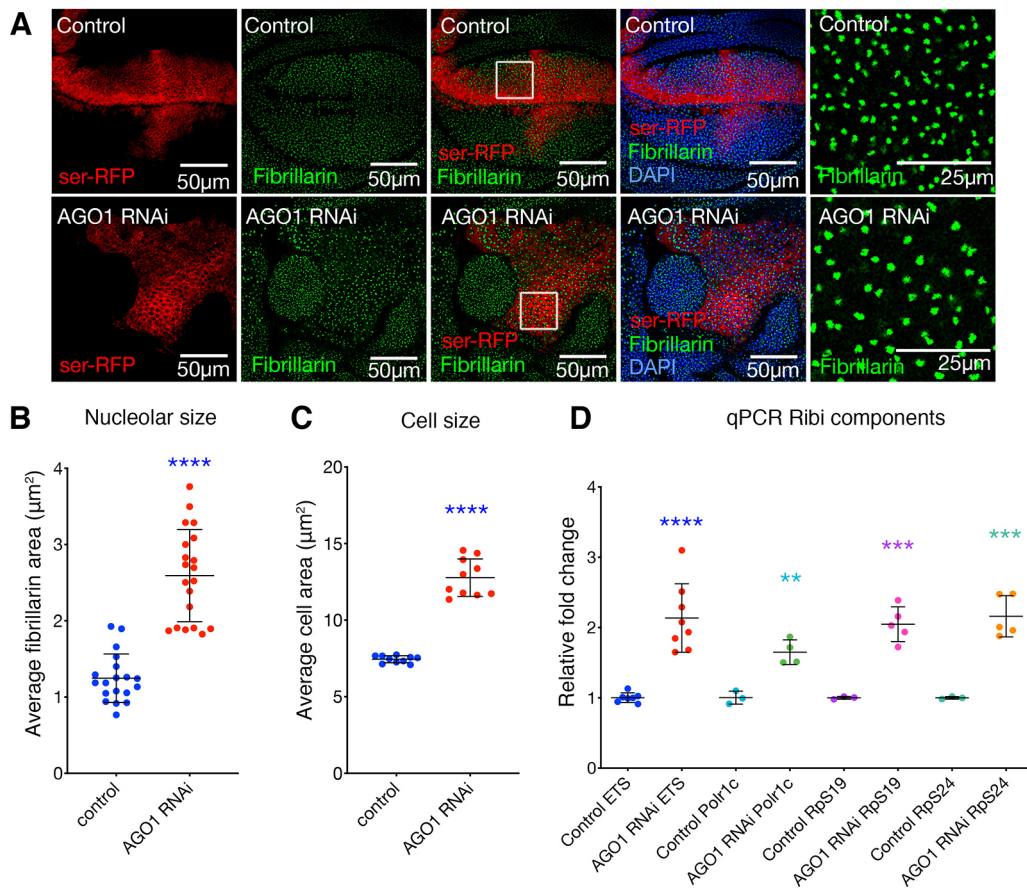


Fig. 3. AGO1 knockdown increases ribosome biogenesis. (A) Third instar wing discs with *ser*-GAL4-driven AGO1 RNAi in the *UAS-p35* background compared with control (*ser*-GAL4, *p35* alone), marked with *UAS-RFP* and stained with anti-fibrillarlin (green) and DAPI (blue). Far right panel shows magnification of the boxed areas. (B) Quantification of average nucleolar area of approximately 50-100 nucleoli within the dorsal compartment, taken from a confocal z-section through the wing discs with *ser*-GAL4 expression in *p35* background (data points are average measurements per image, with mean±s.d. shown). AGO1 RNAi was compared with control. (C) Quantification of cell area marked by CD8-RFP, calculated as average of approximately 50-100 cells per wing disc, in the dorsal compartment of wing *ser*-GAL4 in *p35* background (data points are average measurements per image, with mean±s.d. shown). AGO1 RNAi was compared with control. (D) qPCR for 47S pre-rRNA (ETS), RNA Pol I subunit (*Polr1c*) and ribosomal proteins (*Rps19* and *Rps24*) in wing discs (20 discs pooled for each data point, mean±s.d. shown). Expression was performed for 2 days using *tub*-GAL4 in the background of *tub*-GAL80ts. AGO1 knockdown in the wing significantly increased abundance of *Polr1c*, 47S rRNA 5'-ETS, *Rps19* and *Rps24* ($P=0.0004$ and $P=0.0006$, respectively) compared with the corresponding control. Unpaired two-tailed *t*-test was used for all comparisons. ** $P<0.01$, *** $P<0.001$, **** $P<0.0001$.

knockdown also increased *Psi* mRNA (Fig. 5B) and protein abundance (Fig. S3), suggesting that AGO1 depletion might increase *Myc* (at least in part) by increasing abundance of *Psi*. Together, these data suggest that AGO1 represses *Myc* expression in larval wing discs in a manner partially dependent on *Psi*. In accordance with AGO1 normally being required for *Myc* repression, AGO1 depletion also increased *Myc* protein levels (Fig. 5C). To determine whether increased *Myc* mRNA and protein resulted in heightened *Myc* function (i.e. transcriptional activity) we monitored abundance of two established *Myc* target genes in mammalian and *Drosophila* systems, *Polr1c* (polymerase I polypeptide C) and *Cad* (carbamoyl-phosphate synthase 2) (Mitchell et al., 2015; Poortinga et al., 2014, 2011). *Polr1c* and *Cad* mRNAs were significantly increased following AGO1 depletion, and co-knockdown of *Psi* or *Myc* reduced abundance of these *Myc* target mRNAs (Fig. 5D,E). Together, these data suggest that AGO1 is essential for restraining *Myc* levels and preventing cell overgrowth.

Neither miR-996 nor miR-308 drive *Myc* mRNA turnover

Because AGO1 induces miRNA-dependent mRNA degradation as part of the RISC complex (Hutvagner and Simard, 2008), we tested

whether AGO1 depletion altered *Myc* mRNA levels post transcriptionally. We screened miRBase (Griffiths-Jones, 2004), which contains published mature miRNA sequences from 223 species (Kozomara and Griffiths-Jones, 2014), for miRNAs predicted to target the *Myc* 3'UTR by sequence similarity (<http://www.mirbase.org>). miR-308 and miR-996 were the only miRNAs predicted to target *Myc* (Fig. S4A) that were also expressed in third instar larval tissues based on the modENCODE database (Contrino et al., 2012). In *Drosophila* embryos, miR-308 drives *Myc* mRNA and protein depletion (Daneshvar et al., 2013); however, overexpression of miR-308 did not reduce *Myc* mRNA in the larval wing imaginal disc (Fig. S4B), suggesting that the capacity of miR-308 to target *Myc* depends on the developmental context. In contrast, miR-996 overexpression significantly increased *Myc* mRNA abundance (Fig. S4B), indicating that *Myc* mRNA is not a target for miR-996-driven degradation in the wing. Moreover, the capacity of AGO1 knockdown to increase *Myc* was not altered by overexpression of either miR-308 or miR-996 (Fig. S4B), suggesting that AGO1 repression of *Myc* is not dependent on the function of either of the miRNAs predicted to target *Myc*.

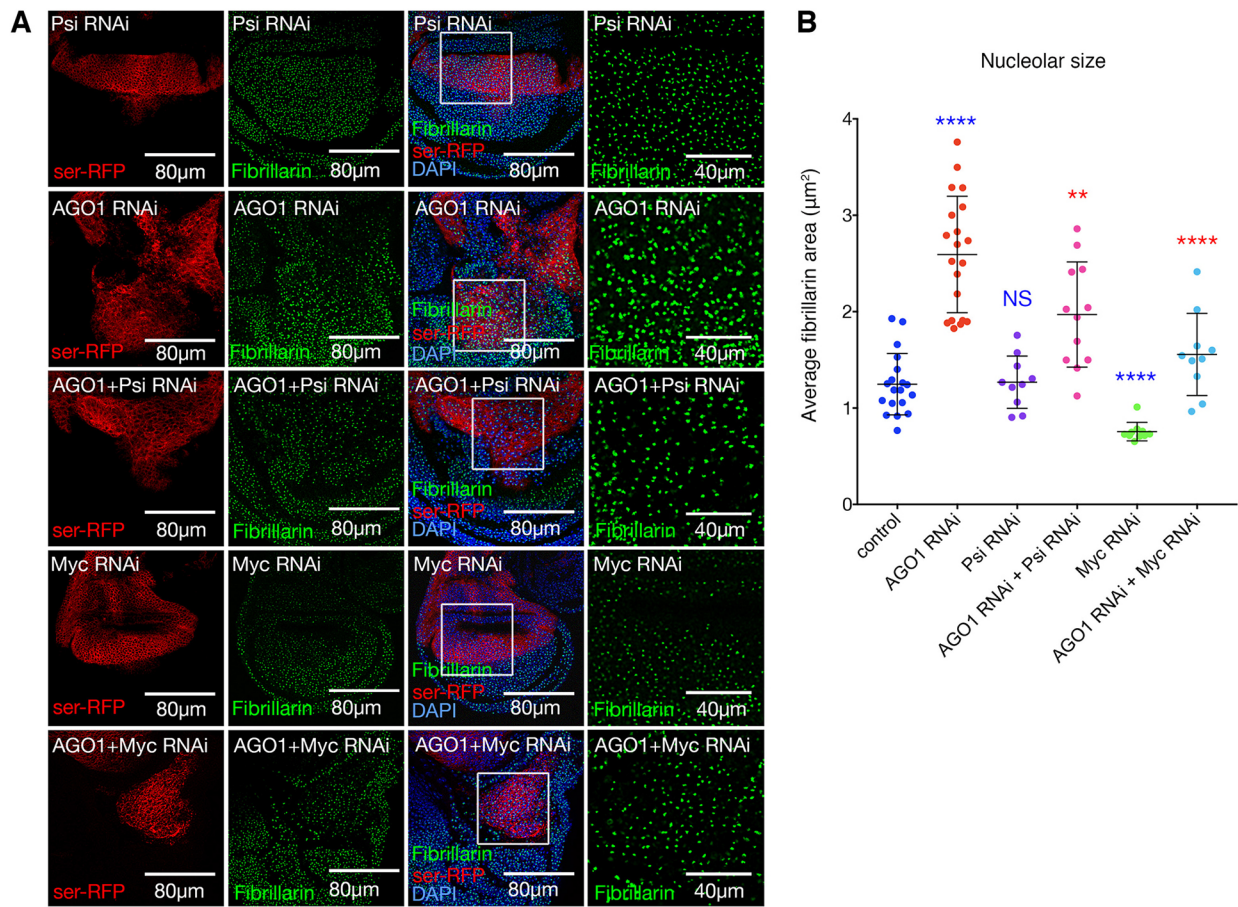


Fig. 4. Increased nucleolar size as a result of AGO1 knockdown is dependent on Psi and Myc. (A) *ser-GAL4*-driven RNAi in RFP-labelled cells for the indicated genotypes in wing discs stained with anti-fibrillarin (green) and DAPI (blue). Far right panel shows magnification of regions in the white squares. (B) Quantification of average nucleolar area of approximately 50-100 nucleoli within the dorsal compartment, taken from a confocal z-section through the wing discs with *ser-GAL4* expression in *p35* background (data points are average measurements per image, mean±s.d. shown). *Myc* RNAi reduced nucleolar size compared with control. Psi or Myc co-depletion significantly reduced nucleolar size in the *AGO1* RNAi background compared with *AGO1* knockdown alone ($P < 0.0001$ and $P = 0.0065$ for Myc and Psi, respectively). Unpaired two-tailed t-test was used for all comparisons. NS, not significant; ** $P < 0.01$, **** $P < 0.0001$.

AGO1 protein localises to the cytoplasm and the nucleus

AGO proteins, together with some components of the RISC, have been reported to enter the nucleus and regulate transcription (Catalanotto et al., 2016; Gosline et al., 2016; Kalantari et al., 2016; Shimada et al., 2016; Thomson et al., 2015; Woolnough et al., 2015). In early stage *Drosophila* blastoderm embryos, AGO1 protein localises to both the nucleus and cytoplasm (Pushpavalli et al., 2012). Biochemical fractionation and confocal immunofluorescence have also detected AGO proteins in the nuclear compartment of mammalian cells (Ahlenstiel et al., 2012). We therefore investigated the localisation of AGO1 in *Drosophila* wing imaginal disc cells using an anti-AGO1 antibody and an AGO1-GFP protein trap, which generates a GFP fusion with endogenous AGO1 (Buszczak et al., 2007). As expected, given miRNA silencing functions, AGO1 and the AGO1-GFP fusion localised predominantly to the cytoplasm in both the wing discs (Fig. 6A,B) and salivary glands (Fig. S5). In addition, co-staining with lamin to mark the nuclear envelope revealed punctate AGO1 staining within the nucleus.

As previous analysis in *Drosophila* antennal discs reported substantial overlap between AGO1 protein and Polycomb (Pc) body foci (42% colocalisation) (Grimaud et al., 2006), we examined whether AGO1 localises to regions of Polycomb group (PcG)

mediated silencing in wing imaginal discs by staining with anti-AGO1 in the Pc-GFP background to mark PcG foci (Dietzel et al., 1999). In contrast to earlier studies using lower resolution microscopy, our high-resolution analysis separated PcG bodies from AGO1 puncta, revealing limited direct overlap (Fig. 6C). Indeed, quantification revealed overlap of just 8% and close proximity of 8.4% between AGO1 and PcG complexes, with the majority (83.6%) of staining occurring independently (Fig. S6A). To confirm that PcG bodies overlap euchromatin, as previously reported (Pirrotta and Li, 2012), DAPI was used to distinguish heterochromatin by intense staining, which revealed both PcG bodies and AGO1 puncta in regions of weaker DAPI staining; that is, AGO1 and PcG localise with euchromatin (Fig. 6C).

The observation that AGO1 puncta and PcG bodies localise to euchromatin, but generally do not directly overlap (83.6%), lends support to the idea that multiprotein and RNA complexes containing AGO1 might serve as a scaffold for assembly of the PcG supercomplexes that underlie both PcG and insulator bodies (Pirrotta and Li, 2012; Shevtsov and Dundr, 2011). Although AGO2 has been reported to enable insulator function independent of RNAi activity through physical association with CTCF binding sites in *Drosophila* (Moshkovich et al., 2011), such roles have not been reported for AGO1. We therefore tested proximity between

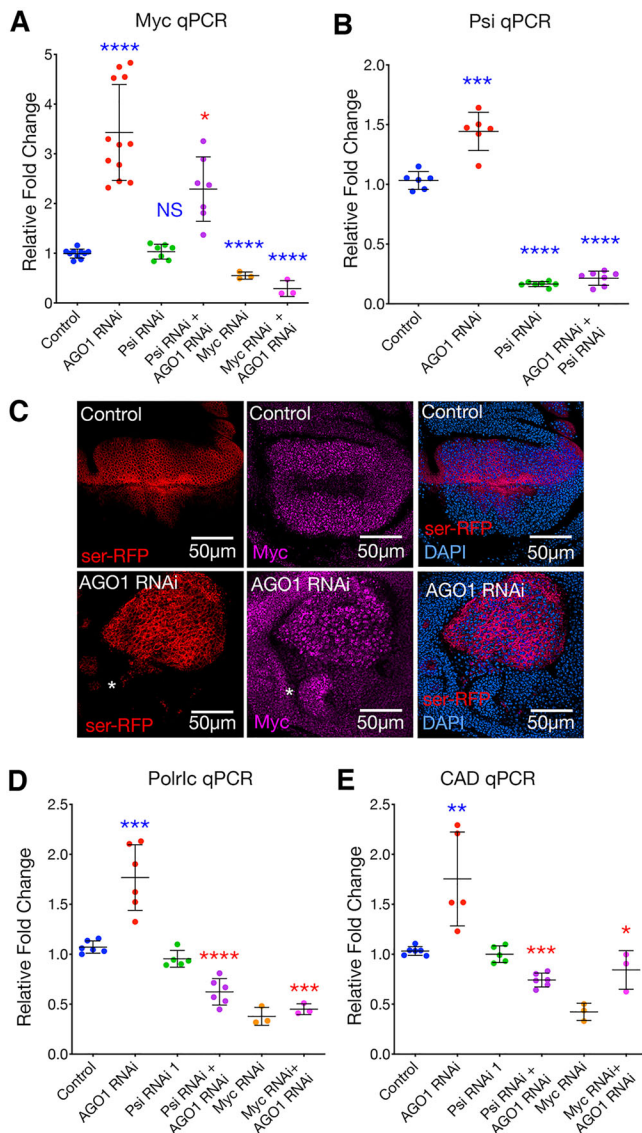


Fig. 5. AGO1 knockdown increases *Myc* abundance and function in larval wing discs. (A) *Myc* qPCR following AGO1 RNAi and/or *Psi* RNAi knockdown (20 discs pooled for each data point, mean \pm s.d. shown). Expression was performed for 2 days using *tub-GAL4* in the background of *tub-GAL80ts*. AGO1 knockdown significantly increased *Myc* mRNA, compared with control. *Psi* co-knockdown significantly reduced *Myc* mRNA compared with AGO1 RNAi alone ($P=0.0134$). *Myc* RNAi, either alone or combined with AGO1 RNAi, significantly decreased *Myc* mRNA compared with control ($P<0.0001$ for both comparisons). (B) *Psi* qPCR for AGO1 RNAi and/or *Psi* RNAi knockdown wing discs (20 discs pooled for each data point, mean \pm s.d. shown). Expression was performed for 2 days using *tub-GAL4* in the background of *tub-GAL80ts*. AGO1 knockdown increased *Psi* mRNA compared with control ($P=0.0002$). *Psi* RNAi, either alone or combined with AGO1 RNAi, significantly decreased *Psi* mRNA compared with control ($P<0.0001$ for both comparisons). (C) Anti-*Myc* antibody (purple) on *ser-GAL4*-driven AGO1 RNAi compared with control. White asterisk indicates a region with elevated *Myc* protein in non-AGO1 knockdown cells. (D,E) qPCR for *Myc*-target genes *Polr1c* (D) and *CAD* (E) in wing discs following AGO1 RNAi and/or *Psi* RNAi knockdown (20 discs pooled for each data point, mean \pm s.d. shown). Expression was performed for 2 days using *tub-GAL4* in the background of *tub-GAL80ts*. AGO1 knockdown significantly increased *Polr1c* and *CAD* mRNA, compared with control ($P=0.0005$ and $P=0.0043$, respectively). *Psi* co-knockdown significantly reduced *Polr1c* and *CAD* mRNA compared with AGO1 RNAi alone ($P<0.0001$ and $P=0.0005$ respectively). *Myc* co-knockdown significantly reduced *Polr1c* and *CAD* mRNA compared with AGO1 RNAi alone ($P=0.0003$ and $P=0.0205$, respectively). Unpaired two-tailed *t*-test was used for all comparisons. NS, not significant; * $P<0.05$, ** $P<0.01$, *** $P<0.001$, **** $P<0.0001$.

AGO1 and chromatin insulator bodies, and the localisation of AGO1 and CTCF chromatin insulator complexes in the nucleus using anti-AGO1 and CTCF-GFP (Fig. 6D). As expected, based on DAPI staining, AGO1 complexes were detected in regions of euchromatin; however, only 15% of the AGO1 puncta were found overlapping or in close proximity with CTCF-marked insulator domains (Fig. 6D; quantified in Fig. S6B). Together these data suggest that AGO1 complexes interact with a small subpopulation of PcG transcriptional silencing loci and CTCF insulator domains in the nucleus.

AGO1 knockdown increases *Myc* transcription

Recent studies demonstrated transcriptional regulation of the *MYC* oncogene involving looping of super-enhancers and that the *MYC* promoter requires a conserved CTCF site (Schuijers et al., 2018). This, together with our observations that AGO1 interacts with the RNA Pol II machinery, localises to euchromatic regions of DNA and overlaps PcG and CTCF complexes, led us to investigate whether AGO1 regulates *Myc* mRNA abundance at the level of transcription. Indeed, AGO1 is required to constrain the *Myc* promoter, as *Myc-lacZ* enhancer trap (Mitchell et al., 2010; Peter et al., 2002) activity was significantly increased in the AGO1 knockdown wing disc compartment (Fig. 7A). To further investigate whether increased *Myc* mRNA associated with AGO1 loss of function was caused by altered transcription, we designed primers to the first intron of *Myc* to measure pre-mRNA levels. Quantitative PCR revealed an increase in the immature *Myc* message following AGO1 knockdown in wing discs (Fig. 7B). Together, these data suggest that the increased *Myc* expression associated with AGO1 depletion is a result of activation of the *Myc* promoter and increased transcription.

Increased *Myc* due to AGO1 depletion requires RNA Pol II transcription

To determine whether AGO1 regulates *Myc* expression at the transcriptional level, we used α -amanitin to block RNA Pol II activity. Consistent with observations using wing imaginal discs (Fig. 5), *Myc* pre- and processed mRNA levels were significantly increased in untreated larval head tissues following AGO1 depletion (Fig. 7C,D). Interestingly, although *Myc* pre-mRNA was significantly decreased 20 and 40 min after α -amanitin treatment (Fig. 7C), mature mRNA was significantly increased in control tissues at the 20 min time point (Fig. 7D), suggesting that *Myc* mRNA stability might increase in response to transcriptional inhibition. In the AGO1 knockdown background, *Myc* pre-mRNA levels were dramatically decreased following α -amanitin treatment (Fig. 7C). Thus, the AGO1 knockdown-induced increase in *Myc* pre-mRNA was dependent on RNA Pol II transcriptional activity. Abundance of the mature *Myc* transcript was not significantly altered in the AGO1 knockdown background following α -amanitin treatment, again suggesting that feedback mechanisms might result in increased mRNA stability in response to RNA Pol II inhibition. Together with the observation that AGO1 knockdown increased *Myc* promoter activity in the wing discs, these data suggest that AGO1 is normally required for repression of *Myc* transcription.

AGO1 is enriched on *Myc*

The increased *Myc* promoter activity following AGO1 depletion, and increased *Myc* mRNA abundance requiring RNA Pol II activity, led us to test whether AGO1 directly regulates *Myc* transcription. We therefore performed ChIP using the anti-AGO1 antibody followed by qPCR with amplicons flanking the *Myc* transcription

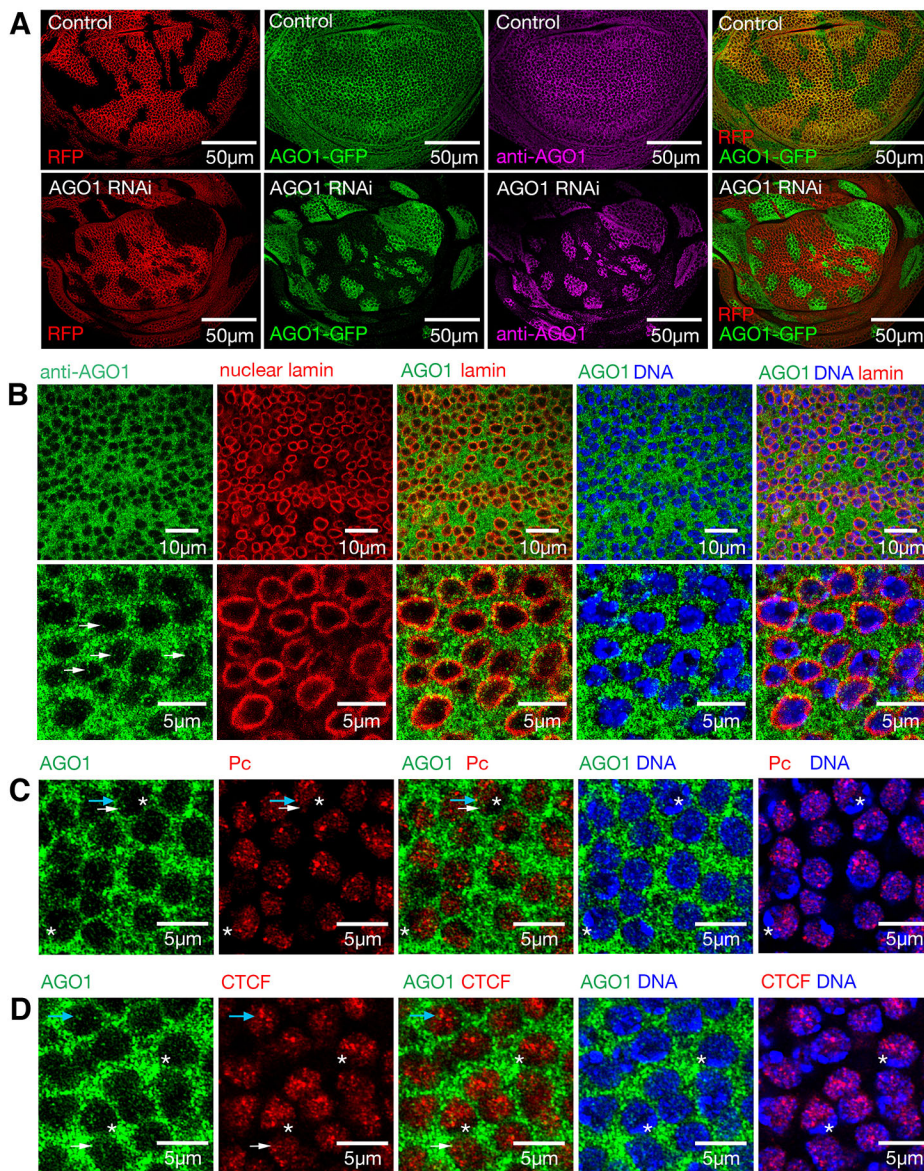


Fig. 6. AGO1 protein localises to both cytoplasmic and nuclear compartments. (A) RFP-marked control and *AGO1* RNAi flip out clones in wing imaginal discs 2 days after heat shock in the *AGO1*-GFP protein trap background, stained with *AGO1* antibody (purple). (B) Wild-type third instar wing imaginal discs stained with *AGO1* antibody (green) and nuclear lamin (red). (C) Single 1 μm z-section from Zeiss Airyscan images for *AGO1* antibody (green) and Pc-GFP (false coloured red). Blue arrow marks *AGO1* puncta with PcG overlap, white arrow marks *AGO1* without clear PcG overlap. Asterisks mark heterochromatin with intense DAPI staining. (D) *AGO1* (green) and CTCF-GFP (false coloured red) for single 1 μm z-sections. Blue arrow marks three *AGO1* puncta, the closest two without CTCF overlap and furthest one with overlap. White arrow marks *AGO1* with weak CTCF overlap. Asterisks mark heterochromatin with intense DAPI staining.

start site (Fig. 7E). In wild-type larval tissues, significant *AGO1* enrichment was observed in *Myc* regulatory regions compared with the mock-IP control, with highest enrichment observed at the transcription start site (Fig. 7F), suggesting that *AGO1* normally inhibits *Myc* transcription through direct interaction with the *Myc* promoter.

DISCUSSION

Here, we demonstrate a novel role for *AGO1* as a growth inhibitor in *Drosophila*. *AGO1* depletion was sufficient to increase *Myc* (mRNA and protein) to drive ribosome biogenesis, nucleolar expansion and cell growth in a *Myc* and *Psi*-dependent manner. The increased *Myc* promoter activity in *AGO1* knockdown wing discs, together with the α -amanitin-dependent increase in *Myc* pre-mRNA abundance, suggests that *AGO1* represses *Myc* at the level of transcription. In accordance with the observed growth inhibitory capacity of *AGO1*, the increased *Myc* mRNA and protein abundance in *AGO1* knockdown wings were associated with increased *Myc* function (i.e. activation of established *Myc* targets). Interestingly, although *Psi* co-knockdown only modestly decreased

Myc mRNA levels in *AGO1*-depleted wings, *Psi* co-depletion strongly reduced expression of *Myc* targets. This observation suggests that *Psi* is not only required for *Myc* transcription (Guo et al., 2016) but may also be required for activation of *Myc* growth targets in the context of *AGO1* depletion. Thus, future studies are required to determine whether *Psi* and *Myc* bind common targets and whether *Psi* is required for transcriptional activation of *Myc* target genes.

Recent genome-wide functional RNAi screens in *Drosophila* S2 cells, identifying *AGO1* as a modifier of Polycomb foci, suggested extra-miRNA functions for *AGO1* (Gonzalez et al., 2014). PcG mediates epigenetic repression of key developmental genes to control cell fate, and PcG repression is stabilised via aggregation of PcG foci in the nucleus. *AGO1* depletion disrupted nuclear organisation and reduced the intensity of Pc foci, suggesting that *AGO1* negatively regulates PcG-mediated silencing (Grimaud et al., 2006). The *Drosophila* PcG complex has been characterised for roles in silencing homeotic genes by binding PcG response elements (PREs), including the Fab-7 PRE-containing regulatory element from the Hox gene, Abdominal-B.

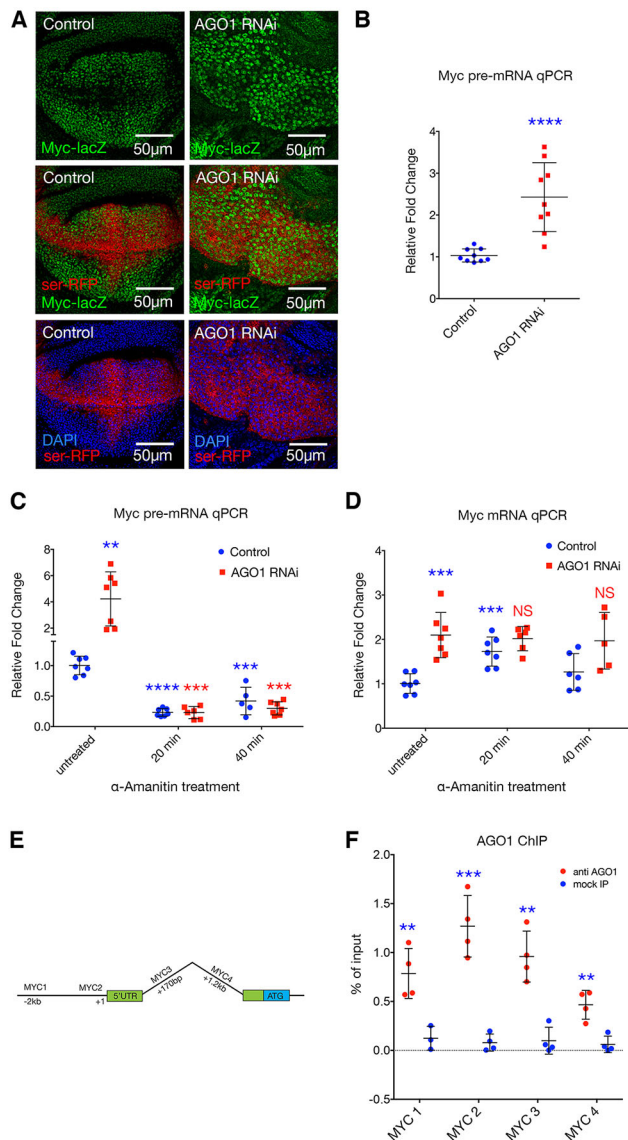


Fig. 7. AGO1 represses *Myc* at the level of transcription. (A) *Myc-lacZ* enhancer trap activity, marked with anti- β -Gal antibody (green) for *ser-GAL4*-driven AGO1 RNAi in the *UAS-p35* background compared with *UAS-p35* alone control, marked with RFP and stained for DNA (blue). (B) qPCR for *Myc* pre-mRNA following AGO1 RNAi knockdown in larval wing discs (20 discs pooled for each data point, mean \pm s.d. shown). Expression was performed for 2 days using *tub-GAL4* in the background of *tub-GAL80ts*. AGO1 RNAi was compared with control. (C) qPCR for *Myc* pre-mRNA following AGO1 knockdown compared with control, performed for 2 days using *tub-GAL4* in the background of *tub-GAL80ts*, in larval head tissues treated with α -amanitin for 20 or 40 min or untreated (five heads pooled for each data point, mean \pm s.d. shown). $P=0.0014$ for untreated AGO1 RNAi compared with untreated control. $P<0.0001$ for 20 min α -amanitin-treated control compared with untreated control. $P=0.0003$ for 40 min α -amanitin-treated control compared with untreated control. $P=0.0006$ for AGO1 RNAi 20 min α -amanitin-treated compared with AGO1 RNAi untreated. $P=0.0003$ for AGO1 RNAi 40 min α -amanitin-treated compared with AGO1 RNAi untreated. (D) qPCR for mature *Myc* mRNA; genotypes and treatment with α -amanitin as described in C. $P=0.0002$ for untreated AGO1 RNAi compared with untreated control. $P=0.0004$ for 20 min α -amanitin treated control compared with untreated control. (E) Schematic of *Myc* showing the position of amplicons used for qPCR. (F) AGO1 ChIP on wild-type larval tissues compared with no-antibody (mock IP) controls ($n=4$ independent experiments, mean \pm s.d. shown). $P=0.0095$ at MYC1, $P=0.0003$ at MYC2, $P=0.0011$ at MYC3 and $P=0.0031$ at MYC4 for AGO1 antibody compared with control. Unpaired two-tailed *t*-test was used for all comparisons. NS, not significant; ** $P<0.01$, *** $P<0.001$, **** $P<0.0001$.

Components of the RNAi machinery, including AGO1 and Dicer-2, have been implicated in driving PcG-dependent silencing between remote copies of the Fab-7 element, engineered throughout the genome to monitor long-distance gene contacts. Interactions between Hox genes silenced by PcG proteins were decreased in AGO1 mutants, suggesting that AGO1 regulates nuclear organisation, at least in part, by stabilising PcG protein recruitment to chromatin (Grimaud et al., 2006).

Myc transcriptional autorepression, modelled in the *Drosophila* embryo via overexpression of *Myc* from an exogenous promoter, leads to repression of the endogenous *Myc* locus in a Pc-dependent manner (Goodliffe et al., 2005). This, together with the partial overlap between AGO1 and PcG in wing imaginal disc cells (Fig. 6C), suggests that Pc mediates transcriptional autorepression of *Myc* via AGO1. In contrast to our studies, where AGO1 depletion phenotypes are associated with a moderate (>three- to fivefold) increase in *Myc*, autoregulation in the embryo was investigated in response to non-physiological increases in *Myc* (over 100 times endogenous levels) (Goodliffe et al., 2005). Thus, our data suggest that AGO1 binds the *Myc* promoter under normal conditions and is required for repression of endogenous *Myc* transcription (Fig. 5A), but whether AGO1 is required for Pc-dependent *Myc* autorepression requires further investigation. In a similar vein, super-enhancers control human *MYC* transcription via CTCF in the context of high-*MYC* cancers (Schuijers et al., 2018). Thus, failed Pc-dependent autorepression and/or defective repression of super-enhancers via CTCF could further elevate *MYC* to promote cancer progression. Given the observed overlap between AGO1 and Pc/CTCF in the *Drosophila* wing, future studies determining whether AGO1 interacts with Pc and/or CTCF to control autoregulatory feedback on *Myc* transcription in the context of tumorigenesis will be of great interest.

The question remains regarding how AGO1 targets *Myc* transcription. The physical and genetic interaction between Psi and AGO1, and the observation that AGO1 loss-of-function mutants restore cell and tissue growth in the Psi knockdown wing, suggests that AGO1 inhibits growth that is dependent on this *Myc* transcriptional regulator. AGO2 has been implicated in insulator-dependent looping interactions defining 3D transcriptional domains (TADs) through association with CTCF binding sites in *Drosophila* (Moshkovich et al., 2011). Although similar roles for AGO1 have not been reported, the cancer-related super-enhancers for the *MYC* oncogene lie within the 2.8 Mb TAD and control *MYC* transcription via a common and conserved CTCF binding site located 2 kb upstream of the *MYC* promoter; that is, in proximity with the FUSE (1.7 kb upstream) bound by FUBP1. Moreover, gene disruption of the enhancer-docking site reduces CTCF binding and super-enhancer interaction, which results in reduced *MYC* expression and proliferative cell growth (Schuijers et al., 2018). AGO1 ChIP revealed significant enrichment on the *Myc* promoter, suggesting that AGO1 probably interacts with Psi and the RNA Pol II machinery to directly regulate *Myc* transcription. Given the high level of conservation between AGO and CTCF proteins throughout evolution, it is of great interest to determine whether human AGO1 also interacts with FUBP1 to regulate transcription of the *MYC* oncogene.

Here, we have shown that AGO1 behaves as a growth inhibitor during *Drosophila* development, through the ability to suppress *Myc* transcription, ribosome biogenesis and cell growth in the wing disc epithelium. Consistent with AGO1 having tumour suppressor activity, across a wide range of human cancers, large scale genomics data in cBioPortal (Gao et al., 2013) identified AGO1 as frequently

mutated or deleted in a diverse variety of tumours (e.g. reproductive, breast, intestinal, bladder, and skin cancers). Region 1p34–35 of chromosome 1, which includes *AGO1*, is frequently deleted in Wilms' tumours and neuro-ectodermal tumours (Parisi et al., 2011). In neuroblastoma cell lines, *AGO1* behaves as a tumour suppressor, with overexpression heightening checkpoint sensitivity and reducing cell cycle progression. GEO Profile microarray data inversely correlates *AGO1* expression with proliferative index (Parisi et al., 2011); that is, *AGO1* levels are significantly lower in tumorigenic cells than in differentiated cells (Barrett et al., 2011). In the context of cancer, it is important to determine whether *AGO1* loss of function alters *MYC*-dependent cancer progression and vice versa. As increased abundance of the *MYC* oncoprotein is associated with the pathogenesis of most human tumours (Dang, 2012; Levens, 2010), deciphering such novel mechanisms of *MYC* repression is fundamental to understanding *MYC*-dependent cancer initiation and progression.

MATERIALS AND METHODS

Drosophila strains

The *UAS-AGO1* RNAi 1 (BL53293), *UAS-AGO1* RNAi 2 (BL33727), *UAS-Myc* (BL9675), *AGO-GFP* (BL50805), *UAS-miR-308* (BL41809), *UAS-miR-996* (BL60653), *Myc-lacZ* (BL12247), *CTCF-GFP* (BL64810), *Pc-GFP* (BL9593), *ser-GAL4* (BL6791), *tub-GAL4* (BL5138), *tub-GAL80ts* (BL7019), *hsflp* (BL1929) and *Act<CD2<GAL4* (BL30558) were obtained from the Bloomington *Drosophila* Stock Center. The *UAS-Myc* RNAi (V2947), *UAS-Psi* RNAi (V105135), *AGO1^{k00208}* (V10470) and *AGO1⁰⁴⁸⁴⁵* (V11388) lines were obtained from the Vienna *Drosophila* RNAi Center.

Co-immunoprecipitation and western blotting

Co-IP was performed using 25 wild-type third instar larval heads dissociated in cold lysis buffer (50 mM Tris pH 7.5, 1.5 mM MgCl₂, 125 mM NaCl, 0.2% NP40, 5% glycerol, 1× protease inhibitor cocktail). Following homogenisation, protein was collected by centrifugation at 13,000 g for 10 min at 4°C. The extract was pre-cleared by incubation with nProtein A Sepharose beads (GE Healthcare Life Science) for 1 h at 4°C with rotation and the supernatant collected by centrifugation at 13,000 g. Equal amounts of pre-cleared protein lysate were incubated with either anti-*AGO1* antibody (Abcam, ab5070, 1:70), anti-*Psi* antibody (custom generated rabbit polyclonal antibody, Biomatik, 1:100) or without antibody (mock IP control) overnight at 4°C. Beads were washed five times with lysis buffer and the eluent resolved using 10% SDS PAGE/western blot with appropriate primary antibody before detection with Li-Cor Odyssey IR.

Immunofluorescence, microscopy and image analysis

Because of the high level of cell death and lethality associated with constitutive *ser-GAL4*-driven *AGO1* depletion, analysis was conducted with co-expressed baculoviral caspase inhibitor p35 to prevent apoptosis (Hay et al., 1994); crosses were maintained at 18°C, unless otherwise stated. Wandering third instar larvae were dissected and fixed for 20 min in 4% paraformaldehyde (PFA), washed in PBS containing 0.1% Tween (PBT), blocked in 5 mg/ml bovine serum albumin (BSA) prior to incubation overnight at 4°C with primary antibody. Primary antibodies used for immunofluorescence were Myc N (rabbit, 1:500; Santa Cruz d46-507), fibrillarin (rabbit, 1:500; Abcam ab5821), *AGO1* (rabbit, 1:500; Abcam ab5070), *Psi* (rabbit, 1:500; custom-made via Biomatik), Lamin (mouse, 1:20; DSHB ADL 101), β-galactosidase (chicken, 1:1000; Abcam ab9361). After incubating with appropriate fluorophore-tagged secondary antibodies (Jackson ImmunoResearch Laboratories; anti-rabbit 488, 1:1000, 711-545-152; anti-chicken 488, 1:1000, 703-485-155; anti-mouse 649, 1:1000, 715-495-151; and anti-rabbit 647, 1:1000, 711-605-152), samples were counterstained with DAPI solution and wing imaginal discs imaged using a Zeiss LSM800 confocal microscope (Zen Blue software). Overlapping 1 μm z-sections were collected at 40× magnification. Fluorophores were imaged

using band-pass filters to remove cross-detection between channels. Images were processed and prepared using ImageJ and Adobe Photoshop CS5. Fibrillarin- and CD8-RFP-marked cell sizes were quantified in FIJI on confocal z-sections of wing columnar epithelial cells, merged to display maximum projections (two or three sections). Thresholding was performed and images were used to measure average fibrillarin area or cell size in the dorsal compartment marked by *serrate-GAL4>UAS-RFP* expression. About 50–100 nucleoli were selected using the freeform selection tool and analysed with the 'Analyse Particles' tool, with minimum particle size of 0.5 μm² applied in order to exclude noise and out-of-focus nucleoli. For cell size, 50–100 cells per wing disc were analysed, with a minimum particle size of 3 μm² applied. The output used image metadata to calculate average area for each wing disc analysed. Analysis of percentage overlap between *AGO1* and *PcG/CTCF* was performed in FIJI by thresholding to isolate individual puncta and overlaying channels to detect co-occurrence or adjacency, which was counted and expressed as a proportion of total *AGO1* puncta per individual nuclei.

Adult wing size analysis

Adult wing size was determined for male wings imaged with an Olympus SZ51 binocular microscope, at 4.5× magnification using the Olympus DP20 camera. Wing size was measured by pixel count for the area posterior to wing vein L5, using Photoshop CS5. For wing hair counts, adult male wings were imaged with an Olympus BX 61 microscope at 20× magnification using the Olympus DP70 camera. Wing cell size was determined using wing hair counts in a defined area (200×100 pixels) at the central region posterior to wing vein L5. Then, the hair number was converted to relative single cell size by dividing the area of the fixed region by hair numbers.

Quantitative PCR

qPCR was performed 2 days after induction of transgene expression using *tub-GAL4* in *tub-GAL80ts* background. RNA was isolated from equivalent numbers of wing imaginal discs (10 pairs for each genotype) using the Promega ReliaPrep RNA Cell miniprep system and eluted in 20 μl nuclease-free water. RNA purity and integrity were assessed using an automated electrophoresis system (2200 TapeStation, Agilent Technologies). Each cDNA synthesis used 6 μl of RNA (GoScript Reverse Transcription System kit, Promega). qPCR was performed using Fast SYBR Green Master Mix (Applied Biosystems) using the StepOnePlus Real-Time PCR System and Sequence Detection Systems in 96-well plates (Applied Biosystems; 95°C for 2 min, 40 cycles 95°C 1 s and 60°C 20 s). Amplicon specificity was verified by melt curve analysis. Average Ct values for two technical replicates were calculated for each sample. Multiple candidate reference genes were analysed for stability across *AGO1* RNAi and control samples using RefFinder. Target gene expression was normalized to the mean of *cyp1* and *tubulin*, selected for having high expression and smallest sample-to-sample variability. Fold change was determined using the 2-ΔΔCT method.

Primers used for qPCR

Myc, 5'-GTGGACGATGGTCCCAATTT-3' and 5'-GGGATTTGTGGG-TAGCTTCTT-3'; Myc pre-mRNA, 5'-TTCAAAATAGAATTTCTGGG-AAAGGT-3' and 5'-GCGGCCATGATCACTGATT-3'; Psi, 5'-CGATGGCATCCCATTTGTTTGT-3' and 5'-GGTGGTCAAGACTACT-CGGC-3'; *AGO1*, 5'-ACTCTACGGTCTGTCCGTTC-3' and 5'-CCCGCTCAGATGCAATCATT-3'; 5'-ETS, 5'-GGCAGTGGTTGCC-GACCTCG-3' and 5'-GCGGAGCCAAGTCCCCTGTT-3'; Tubulin, 5'-TGGGCCCCGTCTGGACCACAA-3' and 5'-TCGCCGTACCCGGAGTC-CAT-3'; *CYP1*, 5'-TCGGCAGCGGCATTTTCAGAT-3' and 5'-TGCACG-CTGACGAAGCTAGG-3'; Polr1c, 5'-TGTATCCCGCCATTGCAA-3' and 5'-GGGCACATCGCTGAGCAT-3'; Cad, 5'-CATTGGCAGTTTCA-AGCACAA-3' and 5'-TCTTGGCCAGATCCCCTATG-3'.

α-Amanitin treatment

α-Amanitin inhibits RNA Pol II-dependent transcription, therefore interfering with mRNA production (Lindell et al., 1970). The α-amanitin (Sigma #A2263) was diluted in 1 ml of Nanopure water to make a 1 mg/ml stock solution, which was stored at -20°C in the dark. Samples were collected 2 days after induction of transgene expression using *tub-GAL4* in

tub-GAL80ts background. Third instar larval heads (anterior imaginal tissues) were dissected and incubated with freshly made 20 µg/ml α-amanitin in Schneider's medium at 25°C for 0, 20 or 40 min. After α-amanitin treatment, samples were washed for 5 min using fresh Schneider's medium and snap frozen in 250 µl LBA+TG lysis buffer from the Promega ReliaPrep RNA Cell Miniprep kit. Following RNA extraction and cDNA synthesis, qPCR was performed and analysed with *Myc* cDNA primers and *Myc* pre-mRNA primers.

Chromatin immunoprecipitation

ChIP assays were carried out as described previously (Lee et al., 2015). Briefly, for each ChIP sample, 30 larval heads were collected from wild-type mid-third instar larvae and fixed in 4% PFA for 20 min. Larval heads were dissociated and chromatin sheared in 0.4% sodium dodecyl sulphate (SDS) using a Covaris S2 (10 min duration, 10% DUTY, 200 cycles per burst, intensity 4, achieving average DNA fragment sizes of 200-600 bp). ChIP was performed in IP buffer containing 0.1% SDS and 3 µg of anti-RNA Pol II phospho-S5 antibody (Abcam, ab5131) or anti-RNA Pol II phospho-S2 (Abcam, ab5095) for each IP. As a control, mock IP was performed without the use of an antibody. Analysis was performed in triplicate using Fast SYBR Green Master Mix (Applied Biosystems) on a StepOnePlus Real-Time PCR System and Sequence Detection Systems in 384-well plates (Applied Biosystems). To calculate the percentage of total DNA bound, non-immunoprecipitated input samples from each condition were used as the qPCR reference for all qPCR reactions.

Primers for ChIP qPCR

The following primers were used for ChIP qPCR: MYC 1, 5'-GGCGATCGTTTCTGGCCTACGG-3' and 5'-GCAGGCGCATTGACTCGGC-3'; MYC 2, 5'-ACTACTACTAACAACTGTCACAAGCCAAGT-3' and 5'-TTATGTATTTGCGCGTTTAAAG-3'; MYC 3, 5'-TTCAAAATAGAA-TTCTGGGAAAGGT-3' and 5'-GCGGCCATGATCACTGATT-3'; MYC 4, 5'-GGTTTTCTTTTATGCCCTTG-3' and 5'-CTATTAACCA-TTGAACCCGAAATC-3'.

Statistical analysis

All statistical tests were performed with Graphpad Prism 6 using an unpaired two-tailed *t*-test with 95% confidence interval. In all figures, error bars represent s.d. and, according to the Graphpad classification of significance points, **P*=0.01-0.05, ***P*=0.001-0.01, ****P*=0.0001-0.001 and *****P*<0.0001.

Acknowledgements

The authors acknowledge the facilities and the scientific and technical assistance of the Centre for Advanced Microscopy and Microscopy Australia at the Advanced Imaging Precinct, Australian National University, a facility that is funded by the University, and State and Federal Governments.

Competing interests

The authors declare no competing or financial interests.

Author contributions

Conceptualization: O.Z., N.C.M., L.G., D.L.L., L.M.Q.; Methodology: O.Z., N.C.M., L.G., L.M.Q.; Validation: O.Z., N.C.M., L.G.; Formal analysis: O.Z., N.C.M., L.G., L.M.Q.; Investigation: O.Z., N.C.M., L.G., O.J.M.; Resources: O.J.M., L.M.Q.; Writing - original draft: O.Z., N.C.M., L.G., D.L.L., L.M.Q.; Writing - review & editing: O.Z., N.C.M., O.J.M., L.M.P., R.D.H., D.L.L., L.M.Q.; Supervision: L.M.P., R.D.H., L.M.Q.; Project administration: L.M.Q.; Funding acquisition: L.M.Q.

Funding

This work was supported by the National Health and Medical Research Council (APP1143008 to L.M.Q.). Deposited in PMC for immediate release.

Supplementary information

Supplementary information available online at <http://dev.biologists.org/lookup/doi/10.1242/dev.190231.supplemental>

Peer review history

The peer review history is available online at <https://dev.biologists.org/lookup/doi/10.1242/dev.190231.reviewer-comments.pdf>

References

- Ahlenstiel, C. L., Lim, H. G. W., Cooper, D. A., Ishida, T., Kelleher, A. D. and Suzuki, K. (2012). Direct evidence of nuclear Argonaute distribution during transcriptional silencing links the actin cytoskeleton to nuclear RNAi machinery in human cells. *Nucleic Acids Res.* **40**, 1579-1595. doi:10.1093/nar/gkr891
- Arabi, A., Wu, S., Ridderstråle, K., Bierhoff, H., Shiu, C., Fatyol, K., Fahlén, S., Hydbring, P., Söderberg, O., Grummt, I. et al. (2005). c-Myc associates with ribosomal DNA and activates RNA polymerase I transcription. *Nat. Cell Biol.* **7**, 303-310. doi:10.1038/ncb1225
- Atwood, B. L., Woolnough, J. L., Lefevre, G. M., Saint Just Ribeiro, M., Felsenfeld, G. and Giles, K. E. (2016). Human Argonaute 2 is tethered to ribosomal RNA through MicroRNA interactions. *J. Biol. Chem.* **291**, 17919-17928. doi:10.1074/jbc.M116.725051
- Barrett, T., Troup, D. B., Wilhite, S. E., Ledoux, P., Evangelista, C., Kim, I. F., Tomashevsky, M., Marshall, K. A., Phillippy, K. H., Sherman, P. M. et al. (2011). NCBI GEO: archive for functional genomics data sets—10 years on. *Nucleic Acids Res.* **39**, D1005-D1010. doi:10.1093/nar/gkq1184
- Buszczak, M., Paterno, S., Lighthouse, D., Bachman, J., Planck, J., Owen, S., Skora, A. D., Nystul, T. G., Ohlstein, B., Allen, A. et al. (2007). The carnegie protein trap library: a versatile tool for Drosophila developmental studies. *Genetics* **175**, 1505-1531. doi:10.1534/genetics.106.065961
- Catalanotto, C., Cogoni, C. and Zardo, G. (2016). MicroRNA in control of gene expression: an overview of nuclear functions. *Int. J. Mol. Sci.* **17**, 1712. doi:10.3390/ijms17101712
- Challagundla, K. B., Sun, X.-X., Zhang, X., DeVine, T., Zhang, Q., Sears, R. C. and Dai, M.-S. (2011). Ribosomal protein L11 recruits miR-24/miRISC to repress c-Myc expression in response to ribosomal stress. *Mol. Cell. Biol.* **31**, 4007-4021. doi:10.1128/MCB.05810-11
- Chung, H. J. and Levens, D. (2005). c-myc expression: keep the noise down! *Mol. Cells* **20**, 157-166.
- Chung, H.-J., Liu, J., Dunder, M., Nie, Z., Sanford, S. and Levens, D. (2006). FBPs are calibrated molecular tools to adjust gene expression. *Mol. Cell. Biol.* **26**, 6584-6597. doi:10.1128/MCB.00754-06
- Contrino, S., Smith, R. N., Butano, D., Carr, A., Hu, F., Lyne, R., Rutherford, K., Kalderimis, A., Sullivan, J., Carbon, S. et al. (2012). modMine: flexible access to modENCODE data. *Nucleic Acids Res.* **40**, D1082-D1088. doi:10.1093/nar/gkr921
- Dalla-Favera, R., Bregni, M., Erikson, J., Patterson, D., Gallo, R. C. and Croce, C. M. (1982). Human c-myc onc gene is located on the region of chromosome 8 that is translocated in Burkitt lymphoma cells. *Proc. Natl. Acad. Sci. USA* **79**, 7824-7827. doi:10.1073/pnas.79.24.7824
- Daneshvar, K., Nath, S., Khan, A., Shover, W., Richardson, C. and Goodliffe, J. M. (2013). MicroRNA miR-308 regulates dMyc through a negative feedback loop in Drosophila. *Biol. Open* **2**, 1-9. doi:10.1242/bio.20122725
- Dang, C. V. (2010). Enigmatic MYC conducts an unfolding systems biology symphony. *Genes Cancer* **1**, 526-531. doi:10.1177/1947601910378742
- Dang, C. V. (2012). MYC on the path to cancer. *Cell* **149**, 22-35. doi:10.1016/j.cell.2012.03.003
- Dietzel, S., Niemann, H., Brückner, B., Maurange, C. and Paro, R. (1999). The nuclear distribution of Polycomb during Drosophila melanogaster development shown with a GFP fusion protein. *Chromosoma* **108**, 83-94. doi:10.1007/s004120050355
- Fernandez, P. C., Frank, S. R., Wang, L., Schroeder, M., Liu, S., Greene, J., Cocito, A. and Amati, B. (2003). Genomic targets of the human c-Myc protein. *Genes Dev.* **17**, 1115-1129. doi:10.1101/gad.1067003
- Förstemann, K., Horwich, M. D., Wee, L. M., Tomari, Y. and Zamore, P. D. (2007). Drosophila microRNAs are sorted into functionally distinct argonaute complexes after production by dicer-1. *Cell* **130**, 287-297. doi:10.1016/j.cell.2007.05.056
- Gao, J., Aksoy, B. A., Dogrusoz, U., Dresdner, G., Gross, B., Sumer, S. O., Sun, Y., Jacobsen, A., Sinha, R., Larsson, E. et al. (2013). Integrative analysis of complex cancer genomics and clinical profiles using the cBioPortal. *Sci. Signal.* **6**, pl1. doi:10.1126/scisignal.2004088
- Gomez-Roman, N., Felton-Edkins, Z. A., Kenneth, N. S., Goodfellow, S. J., Athineos, D., Zhang, J., Ramsbottom, B. A., Innes, F., Kantidakis, T., Kerr, E. R. et al. (2006). Activation by c-Myc of transcription by RNA polymerases I, II and III. *Biochem. Soc. Symp.* **73**, 141-154. doi:10.1042/bss0730141
- Gonzalez, I., Mateos-Langerak, J., Thomas, A., Cheutin, T. and Cavalli, G. (2014). Identification of regulators of the three-dimensional polycomb organization by a microscopy-based genome-wide RNAi screen. *Mol. Cell* **54**, 485-499. doi:10.1016/j.molcel.2014.03.004
- Goodliffe, J. M., Wieschaus, E. and Cole, M. D. (2005). Polycomb mediates Myc autorepression and its transcriptional control of many loci in Drosophila. *Genes Dev.* **19**, 2941-2946. doi:10.1101/gad.1352305
- Gosline, S. J. C., Gurtan, A. M., JnBaptiste, C. K., Bosson, A., Milani, P., Dalin, S., Matthews, B. J., Yap, Y. S., Sharp, P. A. and Fraenkel, E. (2016). Elucidating MicroRNA regulatory networks using transcriptional, post-transcriptional, and Histone modification measurements. *Cell Rep.* **14**, 310-319. doi:10.1016/j.celrep.2015.12.031
- Grandori, C., Gomez-Roman, N., Felton-Edkins, Z. A., Ngouenet, C., Galloway, D. A., Eisenman, R. N. and White, R. J. (2005). c-Myc binds to human ribosomal

- DNA and stimulates transcription of rRNA genes by RNA polymerase I. *Nat. Cell Biol.* **7**, 311-318. doi:10.1038/ncb1224
- Grewal, S. S., Li, L., Orian, A., Eisenman, R. N. and Edgar, B. A.** (2005). Myc-dependent regulation of ribosomal RNA synthesis during Drosophila development. *Nat. Cell Biol.* **7**, 295-302. doi:10.1038/ncb1223
- Griffiths-Jones, S.** (2004). The microRNA registry. *Nucleic Acids Res.* **32**, D109-D111. doi:10.1093/nar/gkh023
- Grimaud, C., Bantignies, F., Pal-Bhadra, M., Ghana, P., Bhadra, U. and Cavalli, G.** (2006). RNAi components are required for nuclear clustering of Polycomb group response elements. *Cell* **124**, 957-971. doi:10.1016/j.cell.2006.01.036
- Guo, L., Zaysteva, O., Nie, Z., Mitchell, N. C., Amanda Lee, J. E., Ware, T., Parsons, L., Luwor, R., Poortinga, G., Hannan, R. D. et al.** (2016). Defining the essential function of FBP/KSRP proteins: Drosophila Psi interacts with the mediator complex to modulate MYC transcription and tissue growth. *Nucleic Acids Res.* **44**, 7646-7658. doi:10.1093/nar/gkw461
- Guruharsha, K. G., Rual, J.-F., Zhai, B., Mintseris, J., Vaidya, P., Vaidya, N., Beekman, C., Wong, C., Rhee, D. Y., Cenaj, O. et al.** (2011). A protein complex network of Drosophila melanogaster. *Cell* **147**, 690-703. doi:10.1016/j.cell.2011.08.047
- Hay, B. A., Wolff, T. and Rubin, G. M.** (1994). Expression of baculovirus P35 prevents cell death in Drosophila. *Development* **120**, 2121-2129.
- He, L., Liu, J., Collins, I., Sanford, S., O'Connell, B., Benham, C. J. and Levens, D.** (2000). Loss of FBP function arrests cellular proliferation and extinguishes c-myc expression. *EMBO J.* **19**, 1034-1044. doi:10.1093/emboj/19.5.1034
- Hutvagner, G. and Simard, M. J.** (2008). Argonaute proteins: key players in RNA silencing. *Nat. Rev. Mol. Cell Biol.* **9**, 22-32. doi:10.1038/nrm2321
- Kalantari, R., Chiang, C.-M. and Corey, D. R.** (2016). Regulation of mammalian transcription and splicing by Nuclear RNAi. *Nucleic Acids Res.* **44**, 524-537. doi:10.1093/nar/gkv1305
- Kozomara, A. and Griffiths-Jones, S.** (2014). miRBase: annotating high confidence microRNAs using deep sequencing data. *Nucleic Acids Res.* **42**, D68-D73. doi:10.1093/nar/gkt1181
- Labourier, E., Adams, M. D. and Rio, D. C.** (2001). Modulation of P-element pre-mRNA splicing by a direct interaction between PSI and U1 snRNP 70K protein. *Mol. Cell* **8**, 363-373. doi:10.1016/S1097-2765(01)00311-2
- Lee, J. E. A., Mitchell, N. C., Zaytseva, O., Chahal, A., Mendis, P., Cartier-Michaud, A., Parsons, L. M., Poortinga, G., Levens, D. L., Hannan, R. D. et al.** (2015). Defective Hfp-dependent transcriptional repression of dMYC is fundamental to tissue overgrowth in Drosophila XPB models. *Nat. Commun.* **6**, 7404. doi:10.1038/ncomms8404
- Levens, D.** (2010). You Don't Muck with MYC. *Genes Cancer* **1**, 547-554. doi:10.1177/1947601910377492
- Liao, D. J. and Dickson, R. B.** (2000). c-Myc in breast cancer. *Endocr. Relat. Cancer* **7**, 143-164. doi:10.1677/erc.0.0070143
- Lindell, T. J., Weinberg, F., Morris, P. W., Roeder, R. G. and Rutter, W. J.** (1970). Specific inhibition of nuclear RNA polymerase II by alpha-amanitin. *Science* **170**, 447-449. doi:10.1126/science.170.3956.447
- Liu, J., Kouzine, F., Nie, Z., Chung, H.-J., Elisha-Feil, Z., Weber, A., Zhao, K. and Levens, D.** (2006). The FUSE/FBP/FIR/TFIIH system is a molecular machine programming a pulse of c-myc expression. *EMBO J.* **25**, 2119-2130. doi:10.1038/sj.emboj.7601101
- Marcu, K. B., Bossone, S. A. and Patel, A. J.** (1992). myc function and regulation. *Annu. Rev. Biochem.* **61**, 809-858. doi:10.1146/annurev.bi.61.070192.004113
- Meyer, N. and Penn, L. Z.** (2008). Reflecting on 25 years with MYC. *Nat. Rev. Cancer* **8**, 976-990. doi:10.1038/nrc2231
- Mitchell, N. C., Johanson, T. M., Cranna, N. J., Er, A. L. J., Richardson, H. E., Hannan, R. D. and Quinn, L. M.** (2010). Hfp inhibits Drosophila myc transcription and cell growth in a TFIIH/Hay-dependent manner. *Development (Cambridge, England)* **137**, 2875-2884. doi:10.1242/dev.049585
- Mitchell, N. C., Tchoubrieva, E. B., Chahal, A., Woods, S., Lee, A., Lin, J. I., Parsons, L., Jastrzebski, K., Poortinga, G., Hannan, K. M. et al.** (2015). S6 Kinase is essential for MYC-dependent rDNA transcription in Drosophila. *Cell. Signal.* **27**, 2045-2053. doi:10.1016/j.cellsig.2015.07.018
- Moshkovich, N., Nisha, P., Boyle, P. J., Thompson, B. A., Dale, R. K. and Lei, E. P.** (2011). RNAi-independent role for Argonaute2 in CTCF/CP190 chromatin insulator function. *Genes Dev.* **25**, 1686-1701. doi:10.1101/gad.16651211
- Okamura, K., Ishizuka, A., Siomi, H. and Siomi, M. C.** (2004). Distinct roles for Argonaute proteins in small RNA-directed RNA cleavage pathways. *Genes Dev.* **18**, 1655-1666. doi:10.1101/gad.1210204
- Oskarsson, T. and Trumpp, A.** (2005). The Myc trilogy: lord of RNA polymerases. *Nat. Cell Biol.* **7**, 215-217. doi:10.1038/ncb0305-215
- Parisi, C., Giorgi, C., Batassa, E. M., Braccini, L., Maresca, G., D'agnano, I., Caputo, V., Salvatore, A., Pietrolati, F., Cogoni, C. et al.** (2011). Ago1 and Ago2 differentially affect cell proliferation, motility and apoptosis when overexpressed in SH-SY5Y neuroblastoma cells. *FEBS Lett.* **585**, 2965-2971. doi:10.1016/j.febslet.2011.08.003
- Peter, A., Schöttler, P., Werner, M., Beinert, N., Dowe, G., Burkert, P., Mourkioti, F., Dentzer, L., He, Y., Deak, P. et al.** (2002). Mapping and identification of essential gene functions on the X chromosome of Drosophila. *EMBO Rep.* **3**, 34-38. doi:10.1093/embo-reports/kvf012
- Pirrota, V. and Li, H.-B.** (2012). A view of nuclear Polycomb bodies. *Curr. Opin. Genet. Dev.* **22**, 101-109. doi:10.1016/j.gde.2011.11.004
- Poortinga, G., Wall, M., Sanij, E., Siwicki, K., Ellul, J., Brown, D., Holloway, T. P., Hannan, R. D. and McArthur, G. A.** (2011). c-MYC coordinately regulates ribosomal gene chromatin remodeling and Pol I availability during granulocyte differentiation. *Nucleic Acids Res.* **39**, 3267-3281. doi:10.1093/nar/gkq1205
- Poortinga, G., Quinn, L. M. and Hannan, R. D.** (2014). Targeting RNA polymerase I to treat MYC-driven cancer. *Oncogene* **34**, 403-412. doi:10.1038/onc.2014.13
- Pushpavalli, S. N. C. V. L., Bag, I., Pal-Bhadra, M. and Bhadra, U.** (2012). Drosophila Argonaute-1 is critical for transcriptional cosuppression and heterochromatin formation. *Chromosome Res.* **20**, 333-351. doi:10.1007/s10577-012-9279-y
- Schuijers, J., Manteiga, J. C., Weintraub, A. S., Day, D. S., Zamudio, A. V., Hnisz, D., Lee, T. I. and Young, R. A.** (2018). Transcriptional dysregulation of MYC reveals common enhancer-docking mechanism. *Cell Rep.* **23**, 349-360. doi:10.1016/j.celrep.2018.03.056
- Shevtsov, S. P. and Dundr, M.** (2011). Nucleation of nuclear bodies by RNA. *Nat. Cell Biol.* **13**, 167-173. doi:10.1038/ncb2157
- Shimada, Y., Mohn, F. and Bühler, M.** (2016). The RNA-induced transcriptional silencing complex targets chromatin exclusively via interacting with nascent transcripts. *Genes Dev.* **30**, 2571-2580. doi:10.1101/gad.292599.116
- Shiue, C.-N., Berkson, R. G. and Wright, A. P. H.** (2009). c-Myc induces changes in higher order rDNA structure on stimulation of quiescent cells. *Oncogene* **28**, 1833-1842. doi:10.1038/onc.2009.21
- Taub, R., Kirsch, I., Morton, C., Lenoir, G., Swan, D., Tronick, S., Aaronson, S. and Leder, P.** (1982). Translocation of the c-myc gene into the immunoglobulin heavy chain locus in human Burkitt lymphoma and murine plasmacytoma cells. *Proc. Natl. Acad. Sci. USA* **79**, 7837-7841. doi:10.1073/pnas.79.24.7837
- Thomson, D. W., Pillman, K. A., Anderson, M. L., Lawrence, D. M., Toubia, J., Goodall, G. J. and Bracken, C. P.** (2015). Assessing the gene regulatory properties of Argonaute-bound small RNAs of diverse genomic origin. *Nucleic Acids Res.* **43**, 470-481. doi:10.1093/nar/gku1242
- Vennstrom, B., Sheiness, D., Zabielski, J. and Bishop, J. M.** (1982). Isolation and characterization of c-myc, a cellular homolog of the oncogene (v-myc) of avian myelocytomatosis virus strain 29. *J. Virol.* **42**, 773-779. doi:10.1128/JVI.42.3.773-779.1982
- Wang, Q., Taliaferro, J. M., Klikaite, U., Hilgers, V., Shaevitz, J. W. and Rio, D. C.** (2016). The PSI-U1 snRNP interaction regulates male mating behavior in Drosophila. *Proc. Natl. Acad. Sci. USA* **113**, 5269-5274. doi:10.1073/pnas.1600936113
- Woolnough, J. L., Atwood, B. L. and Giles, K. E.** (2015). Argonaute 2 binds directly to tRNA genes and promotes gene repression in cis. *Mol. Cell. Biol.* **35**, 2278-2294. doi:10.1128/MCB.00076-15
- Zaytseva, O. and Quinn, L. M.** (2017). Controlling the master: chromatin dynamics at the MYC promoter integrate developmental signaling. *Genes (Basel)* **8**, 118. doi:10.3390/genes8040118
- Zhang, J. and Chen, Q. M.** (2013). Far upstream element binding protein 1: a commander of transcription, translation and beyond. *Oncogene* **32**, 2907-2916. doi:10.1038/onc.2012.350